

Nitrogen partial pressure-dependent Mg concentration, structure, and optical properties of $\text{Mg}_x\text{Zn}_{1-x}\text{O}$ film grown by magnetron sputtering

C.X. Cong, B. Yao,^{a)} Y.P. Xie, and G.Z. Xing

Department of Physics, Jilin University, Changchun 130023, People's Republic of China; and Laboratory of Excited State Processes, Changchun Institute of Optics, Fine Mechanics and Physics, Chinese Academy of Sciences, Changchun 130021, People's Republic of China

B.H. Li, X.H. Wang, Z.P. Wei, Z.Z. Zhang, Y.M. Lv, D.Z. Shen, and X.W. Fan

Laboratory of Excited State Processes, Changchun Institute of Optics, Fine Mechanics and Physics, Chinese Academy of Sciences, Changchun 130021, People's Republic of China

(Received 24 February 2007; accepted 18 July 2007)

$\text{Mg}_x\text{Zn}_{1-x}\text{O}$ films were grown on quartz substrates at 773 K by using radio frequency magnetron sputtering with a mixture of argon and nitrogen as sputtering gases. The nitrogen concentration in the mixture is characterized by the nitrogen partial pressure ratio, which is determined by the ratio of nitrogen flow rate to the flow rates of nitrogen and argon. It was found that Mg concentration, structure, and band gap of the $\text{Mg}_x\text{Zn}_{1-x}\text{O}$ film could be tuned by changing the nitrogen partial pressure ratio of the sputtering gases. The Mg concentration in the $\text{Mg}_x\text{Zn}_{1-x}\text{O}$ film increases with increasing nitrogen partial pressure ratio. The $\text{Mg}_x\text{Zn}_{1-x}\text{O}$ film consists of wurtzite phase at the ratios from 0% to 50%, mixture of wurtzite and cubic phases at the ratios between 50% and 83%, and cubic phase at 100%. The band gap of the $\text{Mg}_x\text{Zn}_{1-x}\text{O}$ film with wurtzite and cubic structure increases as the ratio rises. The variation of the structure and band gap is attributed to change of the Mg concentration, which results from loss of the O and Zn atoms during growth process, the former is induced by reaction between N and O, and the latter by re-evaporation of Zn atoms due to high substrate temperature. The mechanism of the loss of the O and Zn atoms is discussed based on thermodynamics.

I. INTRODUCTION

ZnO has attracted significant attention in the last years for potential applications in ultraviolet (UV) optoelectronic devices, such as light-emitting diodes (LED), laser diodes, and photodetectors, due to its suitable band gap (3.37 eV) and large exciton binding energy (60 meV) at room temperature.^{1–3} In recent years, the success in both controlled *n*-type⁴ as well as *p*-type⁵ doping of ZnO opened the path for optoelectronic device fabrication. Many research groups reported recently that they prepared ZnO *p*-*n* homojunction LED and realized electroluminescence.^{6–8} However, the electroluminescence does not come from recombination of excitons in the UV range but rather by recombination related to defects in visible range, so that visible radiation is dominant in the electroluminescent spectrum. To obtain UV-dominant

electroluminescence, a crucial step is fabrication of ZnO-based LED with a quantum-well active layer or superlattice. A common approach for the preparation of such LEDs would be to develop ZnO-based barrier alloys with band gaps larger than the band gap of ZnO. More recently, a ZnO-based UV LED was fabricated by employment of a quantum-well active layer of composed by barrier alloy of BeZnO and ZnO and emitted UV-dominant spectrum by injection of electric current.⁹ However, techniques used to prepare the BeZnO alloy may be complicated due to safety concerns, and use of such LEDs may introduce health concerns because Be can be poisonous.

Another candidate barrier material is suggested to be $\text{Mg}_x\text{Zn}_{1-x}\text{O}$ alloy, because alloying ZnO with MgO can tune the band gap from 3.37 to 7.8 eV, which is essential for band gap engineering as well as heterostructure device design.¹⁰ Recently, it was reported that near-band-edge emission can be increased and deep-level emission can be suppressed by using $\text{Mg}_x\text{Zn}_{1-x}\text{O}$ as confinement layer in ZnO-based LED, which enabled the confinement

^{a)}Address all correspondence to this author.
e-mail: yaobin196226@yahoo.com.cn
DOI: 10.1557/JMR.2007.0375

of the carrier recombination in the high-quality *n*-type ZnO layer.¹¹ This result indicates that the $\text{Mg}_x\text{Zn}_{1-x}\text{O}$ is a promising candidate barrier material for preparation of LED with UV emission.

Although $\text{Mg}_x\text{Zn}_{1-x}\text{O}$ compounds have been studied extensively in recent years, many key issues still need to be resolved, such as control of Mg concentration, structure, and band gap of $\text{Mg}_x\text{Zn}_{1-x}\text{O}$. In previous reports, these problems were addressed by various methods. Ohtomo et al.¹² and Vashaei et al.¹³ reported that they controlled Mg concentration of the $\text{Mg}_x\text{Zn}_{1-x}\text{O}$ films through changing the Mg content in the target by pulsed-laser deposition and the Mg/Zn flux ratio by plasma-assisted molecular-beam epitaxy, respectively. Bhattacharya et al.¹⁴ obtained $\text{Mg}_x\text{Zn}_{1-x}\text{O}$ films with different Mg concentrations and structures by changing the substrate temperature from 773 to 1023 K. Aside from the reports mentioned above, it seems no other method for modulating Mg content and microstructure of the $\text{Mg}_x\text{Zn}_{1-x}\text{O}$ alloys has been reported up to now. It should be also noted that most studies have focused on the growth, optical, and electrical properties of $\text{Mg}_x\text{Zn}_{1-x}\text{O}$ films^{12,15–17} or $\text{Mg}_x\text{Zn}_{1-x}\text{O}/\text{ZnO}$ superlattices individually.^{18,19} However, reports on the microstructure of $\text{Mg}_x\text{Zn}_{1-x}\text{O}$ films, especially the mechanism of structural variation of $\text{Mg}_x\text{Zn}_{1-x}\text{O}$ films, are currently very limited.

In the present work, $\text{Mg}_x\text{Zn}_{1-x}\text{O}$ films were prepared by using radio frequency (rf) magnetron sputtering technique and mixture of argon and nitrogen as sputtering gases. Differing from previous publications, the Mg content and structure of $\text{Mg}_x\text{Zn}_{1-x}\text{O}$ films were tuned by adjusting the nitrogen partial pressure ratio of the sputtering gases. The mechanism of the variation in the structure and Mg concentration induced by changes in the nitrogen partial pressure ratio is discussed herein on the basis of thermodynamics.

II. EXPERIMENTAL PROCEDURES

$\text{Mg}_x\text{Zn}_{1-x}\text{O}$ films, where *x* is the atomic fraction, were deposited on quartz substrates by rf magnetron sputtering. A disc-shaped $\text{Mg}_{0.18}\text{Zn}_{0.82}\text{O}$ target of 65 mm in diameter and 5 mm in thickness was prepared by sintering mixture of 99.99% pure MgO and ZnO powders at 1273 K for 10 h in an air ambient. The target–substrate distance was 6 cm, and the orientation of the sputter target relative to the substrate is on-axis. A thermocouple was positioned on the reverse side of the substrate holder to measure and control the substrate temperature. The quartz substrates were cleaned in an ultrasonic bath with acetone, ethanol, and deionized water for 15 min sequentially at room temperature, and then washed using deionized water. The growth chamber was evacuated to a base pressure of 5×10^{-4} Pa and then filled with flow of mixed gases (99.99% pure nitrogen and argon) up to

1.0 Pa, and this pressure was maintained during the growing process. The nitrogen concentration in the mixed gases is described by the nitrogen partial pressure ratio, R_{N_2} , which is defined as the nitrogen partial pressure divided by the total pressure of 1.0 Pa, which can be changed from 0% to 100%. The gas pressure ratio can be tuned by controlling flow rates of nitrogen and argon. The deposition time was 1 h, the sputtering power was 100 W, and the growth temperature was 773 K. The as-grown $\text{Mg}_x\text{Zn}_{1-x}\text{O}$ films were annealed for 30 min at 873 K under vacuum conditions of 10^{-4} Pa in a tube furnace. To prevent pollution, a quartz tube was inserted into the furnace and the films were placed in a quartz boat.

The composition of the $\text{Mg}_x\text{Zn}_{1-x}\text{O}$ film was detected by using an energy-dispersive x-ray analyzer (EDX). Film structure was characterized by x-ray diffraction (XRD) with Cu K_α radiation ($\lambda = 0.15406$ nm). The room-temperature absorbance measurement was performed using an UV–VIS–near infrared (NIR) spectrophotometer (Shimadzu, Kyoto, Japan). The thickness of $\text{Mg}_x\text{Zn}_{1-x}\text{O}$ films was measured by scanning electron microscopy (SEM).

III. RESULTS AND DISCUSSION

The crystal structures were identified by XRD for the as-grown and annealed $\text{Mg}_x\text{Zn}_{1-x}\text{O}$ thin films prepared at nitrogen partial pressure ratios ranging from 0% to 100%. The XRD patterns of both as-grown and annealed $\text{Mg}_x\text{Zn}_{1-x}\text{O}$ films are basically the same, except that the 2θ diffraction angles of the as-grown films are smaller than those of annealed films due to existence of tensile stress in the as-grown films. Figure 1 shows the XRD patterns of the annealed $\text{Mg}_x\text{Zn}_{1-x}\text{O}$ thin films grown at various nitrogen partial pressure ratios. As shown in Figs. 1(a) and 1(b), only one diffraction peak is observed at 34.72° and 34.85° , respectively, for the films deposited in pure argon ambient ($R_{\text{N}_2} = 0\%$) and at $R_{\text{N}_2} = 50\%$, indicating that the both films are of wurtzite structure with (002) preferential orientation,

For the $\text{Mg}_x\text{Zn}_{1-x}\text{O}$ films grown at $50\% < R_{\text{N}_2} \leq 83\%$, the XRD patterns of all the samples show two diffraction peaks, as shown in Figs. 1(c)–1(e). Figure 1(c) reveals the XRD pattern of the $\text{Mg}_x\text{Zn}_{1-x}\text{O}$ film grown at $R_{\text{N}_2} = 68\%$, indicating that a weak diffraction peak appears at 42.79° besides the strong (002) diffraction peak of wurtzite $\text{Mg}_x\text{Zn}_{1-x}\text{O}$ located near 34.91° . The weak peak is identified to be (200) diffraction of cubic $\text{Mg}_x\text{Zn}_{1-x}\text{O}$. Figures 1(d) and 1(e) show XRD patterns of the $\text{Mg}_x\text{Zn}_{1-x}\text{O}$ grown at $R_{\text{N}_2} = 78$ and 83% , respectively, and both have a (002) diffraction peak of wurtzite $\text{Mg}_x\text{Zn}_{1-x}\text{O}$ and a (200) diffraction peak of cubic $\text{Mg}_x\text{Zn}_{1-x}\text{O}$. On the basis of the analysis above and the XRD data of Figs. 1(c)–1(d), it is deduced that phase

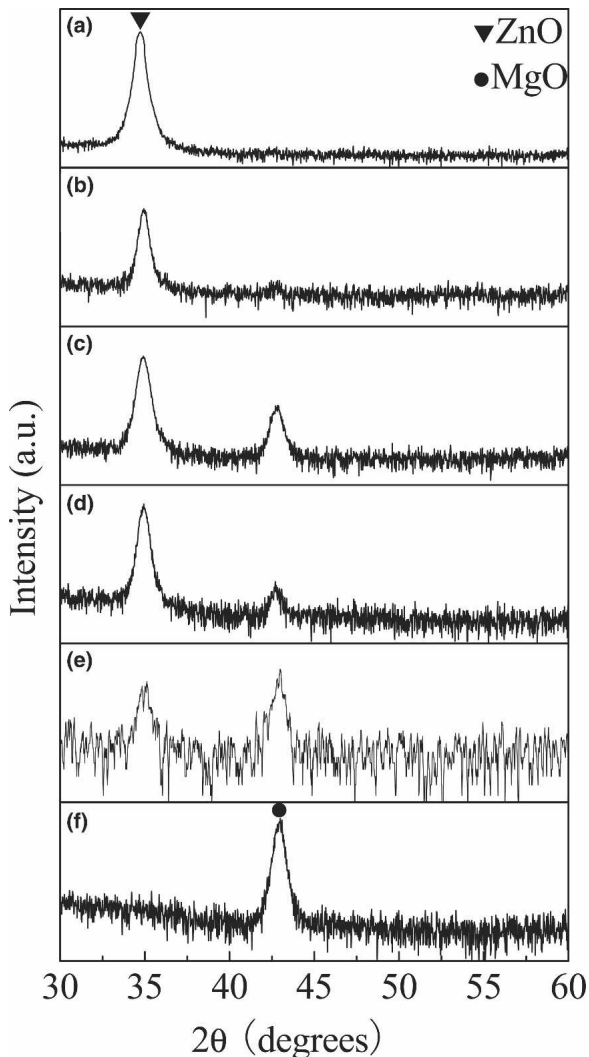


FIG. 1. XRD patterns plotted on a log scale for annealed $Mg_xZn_{1-x}O$ films deposited at nitrogen partial pressure ratios of (a) 0%, (b) 50%, (c) 68%, (d) 78%, (e) 83%, and (f) 100%.

segregation begins to occur in the film grown at $R_{N_2} > 50\%$, and the $Mg_xZn_{1-x}O$ films deposited at $50\% < R_{N_2} \leq 83\%$ consist of wurtzite and cubic phases.

For the annealed $Mg_xZn_{1-x}O$ film grown in pure nitrogen ambient ($R_{N_2} = 100\%$), only a (200) diffraction peak was observed at 42.91° [see Fig. 1(f)], which is smaller than the (200) diffraction angle of pure MgO (43.04°), implying that some Zn^{2+} ions occupy the lattice site of Mg^{2+} to form a single cubic $Mg_xZn_{1-x}O$ with (200) preferential orientation.

To investigate mechanism of the structural variation of $Mg_xZn_{1-x}O$ films, the Mg concentration in the $Mg_xZn_{1-x}O$ film was detected by EDX. Figure 2 reveals the Mg concentration as a function of R_{N_2} for the annealed $Mg_xZn_{1-x}O$ films, showing that the Mg content increases with increasing R_{N_2} . Combining the results of Figs. 1 and 2, it is concluded that the annealed $Mg_xZn_{1-x}O$ film consists of a single wurtzite structure in

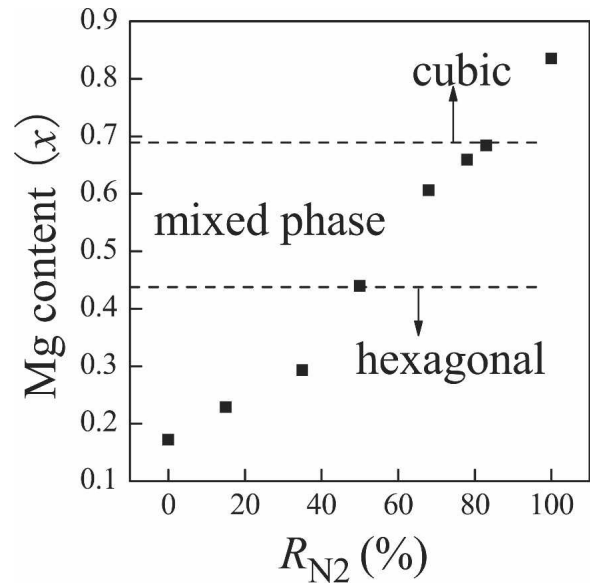


FIG. 2. Plot of Mg concentration as a function of nitrogen partial pressure ratio.

the Mg contents of $0 \leq x < 0.44$, wurtzite and cubic structures between 0.44 and 0.68 and a single cubic structure at $x = 0.83$, that is, the structure of the $Mg_xZn_{1-x}O$ film changes with the Mg concentration.

Lattice constants of the wurtzite and cubic $Mg_xZn_{1-x}O$ were calculated by using the XRD data of Fig. 1, and are plotted as a function of the nitrogen partial pressure ratio in Fig. 3. As Fig. 3 shows, the c -axis lattice constants of the $Mg_xZn_{1-x}O$ with wurtzite structure are all smaller than the value of 0.5209 nm of ZnO powder sample. This is attributed to substitution of some Mg^{2+} for Zn^{2+} in the wurtzite ZnO, because the ionic radius of Mg^{2+} (0.57 Å) is smaller than that of Zn^{2+} (0.60 Å) while the lattice constants of the cubic $Mg_xZn_{1-x}O$ are all larger than the value of 0.42 nm of the MgO powder sample, indicating

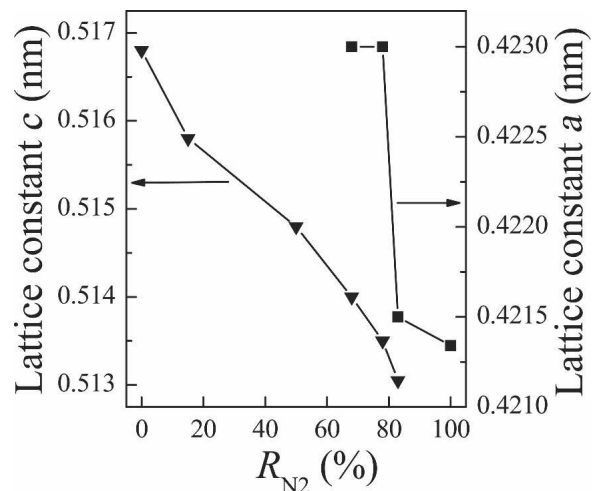


FIG. 3. Lattice constants c and a of annealed $Mg_xZn_{1-x}O$ films as a function of nitrogen partial pressure ratio.

formation of cubic-phase $\text{Mg}_x\text{Zn}_{1-x}\text{O}$. Both the lattice constants c and a decrease with increasing R_{N_2} , indicating that the Mg content in the both wurtzite and cubic $\text{Mg}_x\text{Zn}_{1-x}\text{O}$ increases with increasing R_{N_2} . This is in agreement with results of Fig. 2.

Surface morphology of the $\text{Mg}_x\text{Zn}_{1-x}\text{O}$ film prepared at various R_{N_2} was measured by SEM. Figures 4(a)–4(d) show typical microphotographs of the surface of the $\text{Mg}_x\text{Zn}_{1-x}\text{O}$ films grown at $R_{\text{N}_2} = 0\%$, 50%, 78%, and 100%, respectively, indicating that all the films have a smooth surface and that the grain size decreases with increasing R_{N_2} , in agreement with result calculated using the XRD data and Scherrer's formula.

Figure 5 shows room-temperature absorbance spectra of the $\text{Mg}_x\text{Zn}_{1-x}\text{O}$. Only one absorption edge is observed in the films fabricated at the $R_{\text{N}_2} \leq 50\%$, and the edge shifts to a short-wavelength direction as the R_{N_2} increases. When the nitrogen partial pressure ratio increased to $>50\%$, the absorption curve near the absorption edge became gentle and two absorption edges were observed [Fig. 5(c)], which is a typical absorbance spectrum of $\text{Mg}_x\text{Zn}_{1-x}\text{O}$ film grown at $R_{\text{N}_2} = 78\%$. The two absorption edges are seen clearly when R_{N_2} reaches 83% [Fig. 5(d)]. According to the XRD result of Fig. 1, phase segregation begins occurring in the film grown at

$R_{\text{N}_2} > 50\%$, so it is concluded that the appearance of the two absorption edges is due to the phase segregation, that the absorption edge at low photon energy is for wurtzite $\text{Mg}_x\text{Zn}_{1-x}\text{O}$, and that the absorption edge at high photon energy is for cubic $\text{Mg}_x\text{Zn}_{1-x}\text{O}$. As the R_{N_2} reached 100%, only one absorption edge is observed [see Fig. 5(e)], and the edge shifted far toward the short-wavelength direction. This absorption edge is for cubic $\text{Mg}_x\text{Zn}_{1-x}\text{O}$, based on the result of Fig. 1(f). The results above indicate that the absorption edge (or band gap) of the wurtzite and cubic $\text{Mg}_x\text{Zn}_{1-x}\text{O}$ can be tuned by changing R_{N_2} .

The band gap (E_g) of the wurtzite and cubic $\text{Mg}_x\text{Zn}_{1-x}\text{O}$ is evaluated by employing a $(\alpha/h\nu)^2 \propto (h\nu - E_g)$ relationship and the data of Fig. 5, where α is the absorption coefficient and $h\nu$ is the photon energy. E_g is plotted as a function of Mg concentration in Fig. 6. All the E_g values of the $\text{Mg}_x\text{Zn}_{1-x}\text{O}$ films are larger than the E_g of ZnO (3.37 eV), implying that ZnO alloying with MgO is feasible to enlarge the band gap of ZnO. The E_g increased linearly from 3.64 to 4.09 eV for the single wurtzite $\text{Mg}_x\text{Zn}_{1-x}\text{O}$ as the Mg concentration increases from 0.17 to 0.44, as shown in Fig. 6, indicating that the $\text{Mg}_x\text{Zn}_{1-x}\text{O}$ alloy is a suitable potential barrier layer of a ZnO-based quantum well or superlattice.

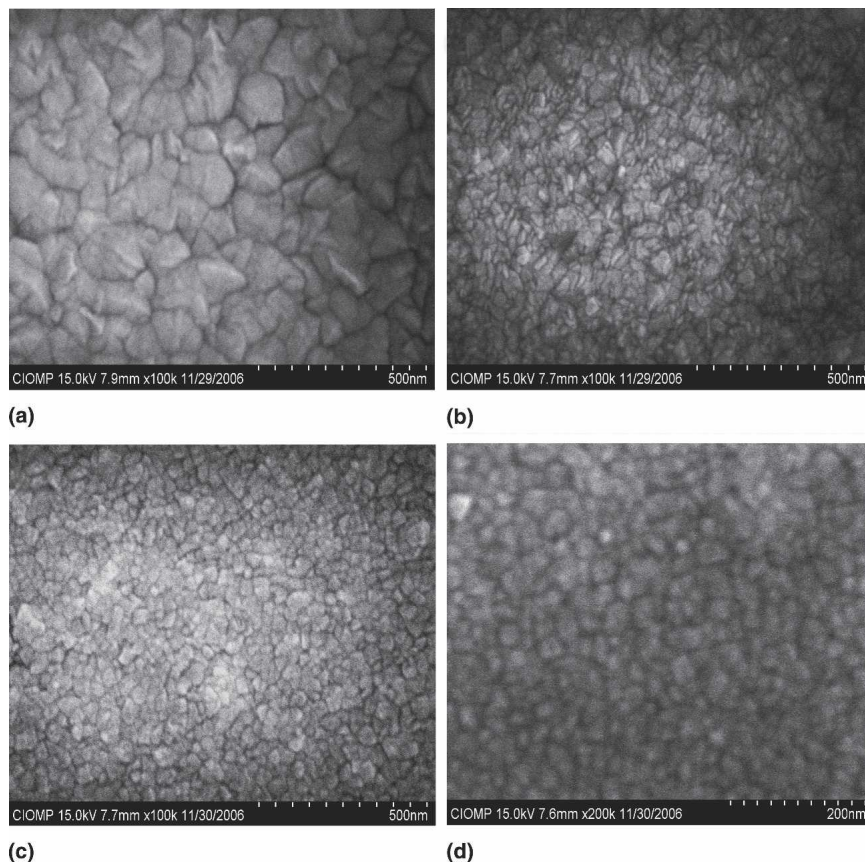


FIG. 4. Typical microphotographs of the surface of the $\text{Mg}_x\text{Zn}_{1-x}\text{O}$ films grown at nitrogen partial pressure ratios of (a) 0%, (b) 50%, (c) 78%, and (d) 100%, respectively.

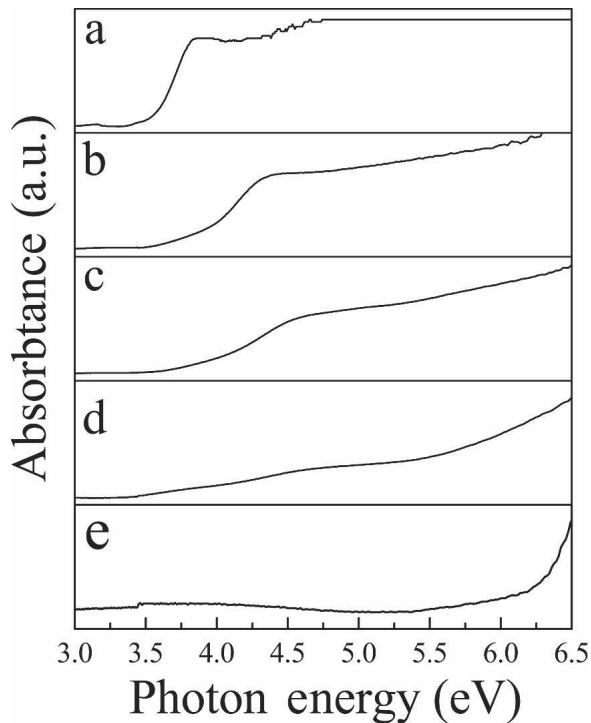


FIG. 5. Relative absorption coefficients of annealed $Mg_xZn_{1-x}O$ films grown at nitrogen partial pressure ratio of (a) 0%, (b) 50%, (c) 78%, (d) 83%, and (e) 100%, respectively.

The results above indicate that the structure and band gap of the $Mg_xZn_{1-x}O$ film can be tuned by the nitrogen partial pressure ratio. The variation of the structure and band gap can be attributed to increase of the Mg concentration in the film with increasing R_{N_2} shown in Fig. 2, according to equilibrium phase diagram of the ternary Mg–Zn–O alloy. However, why does the Mg concentration change with R_{N_2} ? This problem could be explained by reactive thermodynamics.

It is known that the standard enthalpies of formation of NO_2 , MgO , and ZnO are +33.978, –603.96, and –349.02 kJ/mol, respectively, where the negative and positive signs represent exothermic and endothermic reactions, respectively. The bond enthalpies of $N\equiv N$ for N_2 and $O=O$ for O_2 are +944 and +496 kJ/mol, respectively. In the present experiment, the Mg, Zn, and O sources are provided in atom or ion state with the $Mg_{0.18}Zn_{0.82}O$ target sputtered using the gas mixture of Ar and N_2 , and the N source is produced by ionization of N_2 of the mixed gas in a state of atom or ion. Therefore, NO_2 , MgO , and ZnO are formed in the present work by reaction of N, Mg, and Zn atoms or ions with O atoms or ions, respectively, and the enthalpies of formation of the NO_2 , MgO , and ZnO (donated as H_{NO_2} , H_{MgO} , and H_{ZnO} , respectively) in the present experiment are –934, –852, and –597 kJ/mol, respectively, which are calculated by using the standard enthalpies of formation and bond enthalpies mentioned above. Obviously, $H_{NO_2} < H_{MgO} < H_{ZnO}$. Ac-

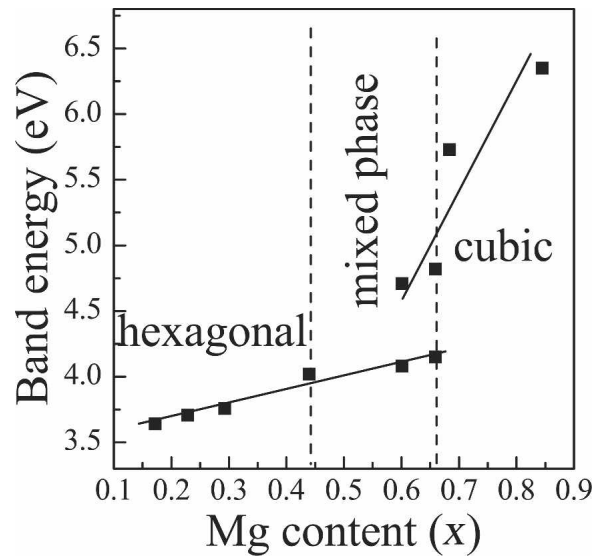
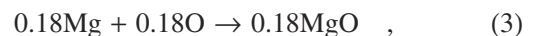
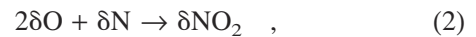
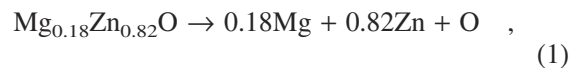


FIG. 6. Plot of band gap of the $Mg_xZn_{1-x}O$ films as a function of Mg content.

ording to the thermodynamic criteria, the N atoms or ions could react preferentially with O atoms or ions to form NO_2 , while most of the NO_2 will be expelled from the growth chamber by pump soon, leading to loss of O atoms. The Mg then reacts with the O to form MgO prior to ZnO due to $H_{MgO} < H_{ZnO}$. Finally the Zn reacts with the remaining O to form ZnO . Because of the loss of O atoms, only some Zn atoms react with O while other Zn atoms become free Zn atoms. These free Zn atoms can deposit on the substrate; however, they will be re-evaporated due to high substrate temperature (773 K) and finally expelled from the growth chamber. As a result, the Mg/Zn atomic ratio in the as-grown Mg–Zn–O film is larger than that in the $Mg_{0.18}Zn_{0.82}O$ target, that is, the Mg concentration in the Mg–Zn–O film is higher than that in the target. The formation process of the Mg–Zn–O can be expressed by following reaction equations:



where δ is the atomic fraction. It is concluded from these four processes that the composition of the as-grown Mg–Zn–O film is $Mg_{(0.18)}Zn_{(0.82-2\delta)}O_{(1-2\delta)}$. The Mg/Zn ratio is equal to $0.18/(0.82 - 2\delta)$. Obviously, as the number of N atoms (δ) increases with R_{N_2} , the Mg/Zn ratio increases with increasing R_{N_2} , which is in agreement with the result of Fig. 2.

On the basis of the discussion above, the loss of Zn and O increases with increasing R_{N_2} , we can deduce that

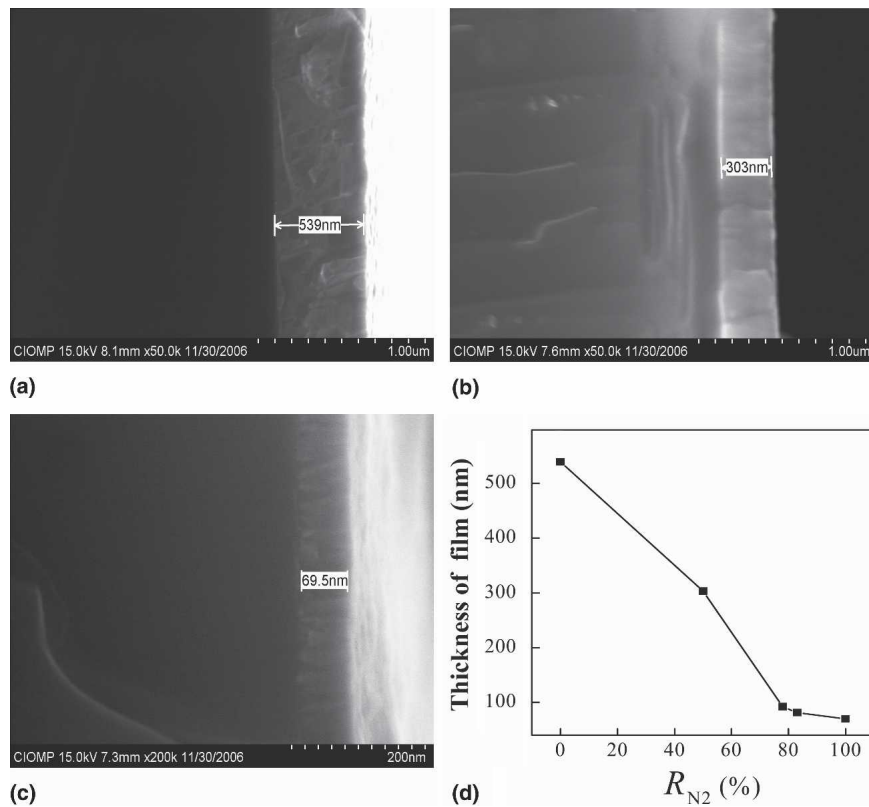


FIG. 7. Typical microphotographs of section of the annealed $Mg_xZn_{1-x}O$ films deposited under nitrogen partial pressure ratios of (a) 0%, (b) 50%, and (c) 100%. (d) Thickness of $Mg_xZn_{1-x}O$ film as a function of nitrogen partial pressure ratio.

the loss of Zn and O leads not only to a decrease in the thickness of the $Mg_xZn_{1-x}O$ film but also to an increase of the Mg concentration with increasing R_{N_2} . In addition, because Ar has a higher sputter yield than N_2 , a decrease of the amount of Ar with increasing R_{N_2} also makes the thickness decrease, but it does not influence Mg concentration in the film. Therefore, the decrease in thickness is attributed to both loss of Zn and O and decrease of sputter yield due to decrease of Ar. To confirm the mechanism mentioned above, the thickness of deposited $Mg_xZn_{1-x}O$ films was measured by SEM. Figures 7(a)–7(c) show typical microphotographs of section of the $Mg_xZn_{1-x}O$ film deposited at various nitrogen partial pressure ratios, from which the thicknesses of the $Mg_xZn_{1-x}O$ films were measured and plotted as a function of R_{N_2} in Fig. 7(d). Figure 7(d) shows that the thickness of the $Mg_xZn_{1-x}O$ film decreases with increasing R_{N_2} , which is consistent with the deduction mentioned above, also demonstrating that the variation of the Mg concentration with R_{N_2} is due to loss of Zn and O.

To demonstrate the effect of substrate temperature on re-evaporation of Zn deposited on the substrate in the $Mg_xZn_{1-x}O$ growth process, Mg/Zn ratio was measured for the $Mg_xZn_{1-x}O$ films deposited at $R_{N_2} = 78\%$ at substrate temperature ranging from 300 to 773 K and plotted as a function of the substrate temperature in Fig.

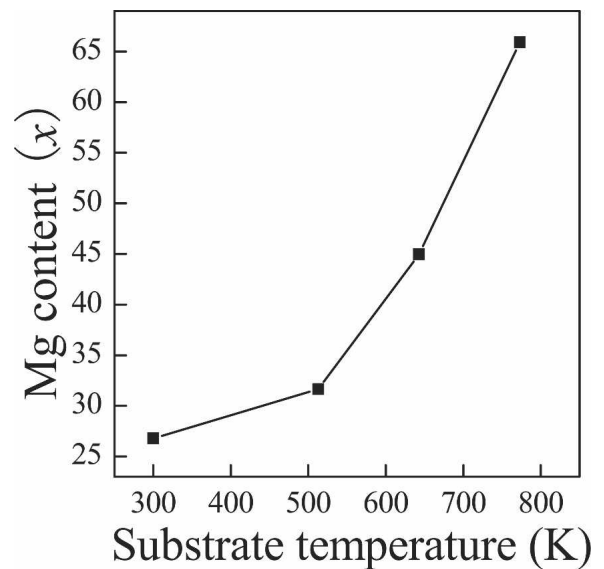


FIG. 8. Plot of Mg concentration as a function of substrate temperature.

8. Figure 8 shows that the Mg/Zn ratio increases with increasing the substrate temperature, indicating that the number of lost Zn atoms increases with increasing substrate temperature. The result of Fig. 8 implies that some excessive Zn atoms unreacted with O atoms are re-evaporated as they deposit on the substrate in the

Mg_xZn_{1-x}O growth process and pumped out from the chamber, leading to loss of Zn atoms and a decrease of Mg/Zn ratio. The higher the substrate temperature, the greater the loss of Zn atoms.

The results of Figs. 7 and 8 confirm the mechanism of change of structure and properties of the Mg_xZn_{1-x}O films with R_{N_2} suggested above.

The mechanism is also confirmed by our other experiments, where Mg_xZn_{1-x}O films were grown by sputtering the Mg_{0.18}Zn_{0.82}O target with a mixture of N₂ and O₂. Only a Mg_xZn_{1-x}O film with wurtzite structure was obtained as nitrogen partial pressure ratio is <100%, and no structural variation was observed. That is attributed to the loss of O atoms from the target due to reaction with N atoms, which can be compensated for by ionization of the O₂ in the mixed gases so that there are enough O atoms to react with Mg and Zn to form Mg_xZn_{1-x}O alloy in the growth process.

IV. CONCLUSIONS

Mg_xZn_{1-x}O films with different Mg concentrations, structures, and band gaps were fabricated by sputtering the Mg_{0.18}Zn_{0.82}O target with mixture of Ar and N₂. The Mg concentration, structure, and band gap of the Mg_xZn_{1-x}O films can be tuned by changing the nitrogen partial pressure ratio. The Mg concentration increases as the nitrogen partial pressure ratio increases. The Mg_xZn_{1-x}O film consists of wurtzite phase in the range of $0\% \leq R_{N_2} \leq 50\%$, a mixture of wurtzite and cubic phases in the range of $50\% < R_{N_2} \leq 83\%$, and cubic phase at 100%. The band gaps of both wurtzite and cubic Mg_xZn_{1-x}O films increase with increasing R_{N_2} . The changes of the structure and band gap with the nitrogen partial pressure are due to variation of the Mg content with the R_{N_2} . Although the variation of Mg concentration is mainly attributed to the loss of the O and Zn atoms, the former is induced by reaction between N and O, and the latter results from some excessive Zn atoms being re-evaporated as they deposit on the substrate due to high substrate temperature and expelled from the chamber.

ACKNOWLEDGMENTS

The authors appreciate financial support of Key Projects of the National Natural Science Foundation of China (Grants 60336020 and 50532050) and the National Natural Science Foundation of China (Grant No. 50472003).

REFERENCES

1. D.C. Look: Recent advances in ZnO materials and devices. *Mater. Sci. Eng., B* **80**, 383 (2001).
2. Z.K. Tang, G.K.L. Wong, P. Yu, M. Kawasaki, A. Ohtomo, H. Koinuma, and Y. Segawa: Room-temperature ultraviolet laser emission from self-assembled ZnO microcrystallite thin films. *Appl. Phys. Lett.* **72**, 3270 (1998).
3. A. Ohtomo, K. Tamura, and M. Kawasaki: Room-temperature stimulated emission of excitons in ZnO/(Mg, Zn)O superlattices. *Appl. Phys. Lett.* **77**, 2204 (2000).
4. T. Makino, K. Tamura, C.H. Chia, Y. Segawa, M. Kawasaki, A. Ohtomo, and H. Koinuma: Optical properties of ZnO Al epilayers and of undoped epilayers capped by wider-gap Mg_xZn_{1-x}O grown by laser MBE. *Phys. Status Solidi B* **229**, 853 (2002).
5. S. Choopun, R.D.W. Vispute, A. Noch, R.P. Balsamo, T. Sharma, A.V. Iliadis, and D.C. Look: Oxygen pressure-tuned epitaxy and optoelectronic properties of laser-deposited ZnO films on sapphire. *Appl. Phys. Lett.* **75**, 3947 (1999).
6. A. Tsukazaki, A. Ohtomo, T. Onuma, M. Ohtani, T. Makino, M. Sumiya, K. Ohtani, S.F. Chichibu, S. Fuke, Y. Segawa, H. Ohno, H. Koinuma, and M. Kawasaki: Repeated temperature modulation epitaxy for *p*-type doping and light-emitting diode based on ZnO. *Nat. Mater.* **4**, 42 (2005).
7. S.J. Jiao, Z.Z. Zhang, Y.M. Lu, D.Z. Shen, B. Yao, J.Y. Zhang, B.H. Li, D.X. Zhao, X.W. Fan, and Z.K. Tang: ZnO *p-n* junction light-emitting diodes fabricated on sapphire substrates. *Appl. Phys. Lett.* **88**, 031911 (2006).
8. M.-C. Jeong, B.-Y. Oh, M.-H. Ham, and J.-M. Myoung: Electroluminescence from ZnO nanowires in *n*-ZnO film/ZnO nanowire array/*p*-GaN film heterojunction light-emitting diodes. *Appl. Phys. Lett.* **88**, 202105 (2006).
9. Y. Ryu, T.-S. Lee, J.A. Lubguban, H.W. White, B.-J. Kim, Y.-S. Park, and C.-J. Youn: Next generation of oxide photonic devices: ZnO-based ultraviolet light emitting diodes. *Appl. Phys. Lett.* **88**, 241108 (2006).
10. Y. Matsumoto, M. Murakami, Z. Jin, and A. Ohtomo: Combinatorial laser molecular beam epitaxy (MBE) growth of Mg-Zn-O alloy for band gap engineering. *Jpn. J. Appl. Phys.* **38**(2), L603 (1999).
11. J.-H. Lim, C.-K. Kang, K.-K. Kim, I.-K. Park, D.-K. Hwang, and S.-J. Park: UV electroluminescence emission from ZnO light-emitting diodes grown by high-temperature radiofrequency sputtering. *Adv. Mater.* **18**, 2720 (2006).
12. A. Ohtomo, M. Kawasaki, T. Koida, K. Masubuchi, H. Koinuma, Y. Sakurai, Y. Segawa, T. Yasuda, and Y. Segawa: Mg_xZn_{1-x}O as a II-VI widegap semiconductor alloy. *Appl. Phys. Lett.* **72**(19), 2466 (1998).
13. Z. Vashaei, T. Minegishi, H. Suzuki, T. Hanada, M.W. Cho, and T. Yao: Structural variation of cubic and hexagonal Mg_xZn_{1-x}O layers grown on MgO(111)/*c*-sapphire. *J. Appl. Phys.* **98**, 054911 (2005).
14. P. Bhattacharya, R. Rasmi, and R.S. Katiyar: Fabrication of stable wide-band-gap ZnO/MgO multilayer thin films. *Appl. Phys. Lett.* **83**(10), 2010 (2003).
15. S. Choopun, R.D. Vispute, W. Yang, R.P. Sharma, T. Venkatesan, and H. Shen: Realization of band gap above 5.0 eV in metastable cubic-phase Mg_xZn_{1-x}O alloy films. *Appl. Phys. Lett.* **80**, 1529 (2002).
16. F.K. Shan, B.I. Kim, G.X. Liu, Z.F. Liu, J.Y. Sohn, W.J. Lee, B.C. Shin, and Y.S. Yu: Blueshift of near-band-edge emission in Mg doped ZnO thin films and aging. *J. Appl. Phys.* **95**(9), 4772 (2004).
17. H.S. Kang, G.H. Kim, D.L. Kim, H.W. Chang, B.D. Ahh, and S.Y. Lee: Investigation on the *p*-type formation mechanism of arsenic doped *p*-type ZnO thin film. *Appl. Phys. Lett.* **89**, 181103 (2006).
18. A. Ohtomo, K. Tamura, M. Kawasaki, T. Makino, Y. Segawa, Z.K. Tang, G.K.L. Wong, Y. Matsumoto, and H. Koinuma: Room-temperature stimulated emission of excitons in ZnO/(Mg,Zn)O superlattices. *Appl. Phys. Lett.* **77**(14), 2204 (2000).
19. Th. Gruber, C. Kirchner, R. Kling, F. Reuss, and A. Waag: ZnMgO epilayers and ZnO-ZnMgO quantum wells for optoelectronic applications in the blue and UV spectral region. *Appl. Phys. Lett.* **84**(26), 5359 (2004).